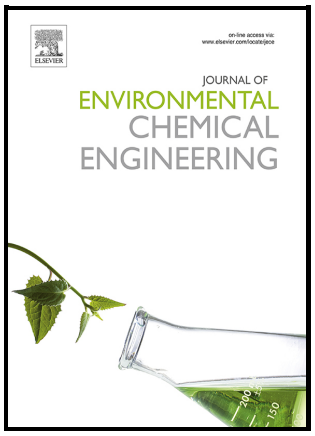

Synergistic Effects of Catalytic Co-Pyrolysis *Chlorella vulgaris* and Polyethylene Mixtures using Artificial Neuron Network: Thermodynamic and Empirical Kinetic Analyses

Tshun Li Yap, Adrian Chun Minh Loy, Bridgid Lai Fui Chin, Juin Yau Lim, Hatem Alhamzi, Yee Ho Chai, Chung Loong Yiin, Kin Wai Cheah, Melvin Xin Jie Wee, Man Kee Lam, Zeinab Abbas Jawad, Suzana Yusup, Serene Sow Mun Lock

PII: S2213-3437(22)00264-0

DOI: https://doi.org/10.1016/j.jece.2022.107391

Reference: JECE107391

To appear in: *Journal of Environmental Chemical Engineering*

Received date: 21 November 2021
Revised date: 26 January 2022
Accepted date: 11 February 2022

Please cite this article as: Tshun Li Yap, Adrian Chun Minh Loy, Bridgid Lai Fui Chin, Juin Yau Lim, Hatem Alhamzi, Yee Ho Chai, Chung Loong Yiin, Kin Wai Cheah, Melvin Xin Jie Wee, Man Kee Lam, Zeinab Abbas Jawad, Suzana Yusup and Serene Sow Mun Lock, Synergistic Effects of Catalytic Co-Pyrolysis *Chlorella vulgaris* and Polyethylene Mixtures using Artificial Neuron Network: Thermodynamic and Empirical Kinetic Analyses, *Journal of Environmental Chemical Engineering,* (2021) doi:https://doi.org/10.1016/j.jece.2022.107391

Synergistic Effects of Catalytic Co-Pyrolysis *Chlorella vulgaris* and Polyethylene Mixtures using Artificial Neuron Network: Thermodynamic and Empirical Kinetic Analyses

Tshun Li Yap[a], Adrian Chun Minh Loy[b,c,d], Bridgid Lai Fui Chin[a]*, Juin Yau Lim[e], Hatem Alhamzi[f], Yee Ho Chai[c,d], Chung Loong Yiin[g], Kin Wai Cheah[h], Melvin Xin Jie Wee[a], Man Kee Lam[c,d], Zeinab Abbas Jawad[i], Suzana Yusup[j], Serene Sow Mun Lock[k]

[a]Department of Chemical and Energy Engineering, Faculty of Engineering and Science, Curtin University Malaysia, CDT 250, 98009 Miri Sarawak, Malaysia.

E-mail: (1) 700017566@student.curtin.edu.my (Tshun Li Yap)

(2) bridgidchin@curtin.edu.my / bridgidchin@gmail.com (Dr Bridgid Lai Fui Chin)*

(3) melvinweexj@postgrad.curtin.edu.my (Melvin Xin Jie Wee)

*Corresponding author

[b]Department of Chemical Engineering, Monash University, Victoria, 3800, Australia

E-mail: (1) adrian.loy@monash.edu

[c]HICoE - Centre for Biofuel and Biochemical Research, Institute of Self-Sustainable Building, Department of Chemical Engineering, Universiti Teknologi PETRONAS, 32610, Seri Iskandar, Perak.

E-mail: (1) yeeho.chai@utp.edu.my (Dr Yee Ho Chai)

(2) lam.mankee@utp.edu.my (Dr Man Kee Lam)

[d]Department of Chemical Engineering, Universiti Teknologi PETRONAS, 32610 Seri Iskandar, Perak, Malaysia.

[e]Integrated Engineering, Dept. of Environmental Science and Engineering, College of Engineering, Kyung Hee University, 1732 Deogyeong-daero, Giheung-gu, Yongin-Si, Gyeonggi-do 17104, Republic of Korea.

E-mail: juinyau95@gmail.com

[f]National Center for Environmental Technology (NCET), King Abdulaziz City for Science and Technology (KACST), P.O. Box 6086, 11442 Riyadh, Saudi Arabia.
E-mail: halhazmi@kacst.edu.sa

[g]Department of Chemical Engineering and Energy Sustainability, Faculty of Engineering, Universiti Malaysia Sarawak (UNIMAS), 94300, Kota Samarahan, Sarawak, Malaysia.
E-mail: clyiin@unimas.my

[h]Teesside University, School of Science and Engineering Borough Road, Middlesbrough TS1 3BA, United Kingdom.
E-mail: cheahkinwai@hotmail.com

[i]Department of Chemical Engineering, College of Engineering, Qatar University, P.O. Box: 2713, Doha, Qatar.
E-mail: zjawad@qu.edu.qa

[j]Generation Unit (Fuel Technology & Combustion), Tenaga Nasional Berhad (TNB) Research Sdn Bhd, No.1, Kawasan Institusi Penyelidikan, Jln Ayer Hitam, 43000 Kajang, Selangor.
E-mail: suzana.yusup@tnb.com.my

[k]CO_2 Research Center (CO_2 RES), Department of Chemical Engineering, Universiti Teknologi PETRONAS, Seri Iskandar 32610, Malaysia.
E-mail: sowmun.lock@utp.edu.my

Keywords: Catalytic pyrolysis, Kinetic analysis, Empirical modelling, Artificial neural network, Genetic algorithm, Microalgae *Chlorella vulgaris*

Abstract

The catalytic pyrolysis of *Chlorella vulgaris*, high-density polyethylene (Pure HDPE) and, their binary mixtures were conducted to analyse the kinetic and thermodynamic performances

from 10 – 100 K/min. The kinetic parameters were computed by substituting the experimental and ANN predicted data into these iso-conversional equations and plotting linear plots. Among all the iso-conversional models, Flynn-Wall-Ozawa (FWO) model gave the best prediction for kinetic parameters with the lowest deviation error (2.28-12.76 %). The bifunctional HZSM-5/LS catalysts were found out to be the best catalysts among HZSM-5 zeolite, natural limestone (LS), and bifunctional HZSM-5/LS catalyst in co-pyrolysis of binary mixture of *Chlorella vulgaris* and HDPE, in which the E_a of the whole system was reduced from range 144.93–225.84 kJ/mol (without catalysts) to 75.37–76.90 kJ/mol. With the aid of artificial neuron network and genetic algorithm, an empirical model with a mean absolute percentage error (MAPE) of 51.59% was developed for tri-solid state degradation system. The developed empirical model is comparable to the thermogravimetry analysis (TGA) experimental values alongside the other empirical model proposed in literature.

1.0 Introduction

Energy plays an irreplaceable role in human's daily lives for centuries and also being regarded as the main principal factor for a country's socio-economic development. According to the International Energy Agency (IEA), the total world's energy from non-renewable fossil fuels is experiencing a decline trend due to the emergence of renewable energies (Hossain et al., 2018). In contrast, the use of biomass as alternative energy has come into interest due to its advantages of highly abundant, affordability, sustainability as compared to fossil fuels (Alhazmi & Loy, 2021). Based on the latest renewable energy market analysis from International Energy Agency (IEA) (2019), the biofuel usage will accommodate 25% of the total renewable energy in the year of 2024 due to large investments from stakeholders, specifically in China and Brazil. Microalgae, a third generation of biofuel, the unicellular microorganisms which are rich in carbohydrates and lipid contents has been discovered as an excellent biofuel source. Among the wide variety of microalgae species, *Chlorella vulgaris*

(*C. vulgaris*) has been reported to be a potential candidate for bioenergy production due to its high lipid accumulation, able to cultivate in stress conditions and rapid and perennial growth (Jeong & Kim, 2021; Monjed, Achour, Robson, & Pittman, 2021).

On the other hand, enormous plastic waste production is another one of the most pressing global environmental issues, as rapidly increasing production of disposable plastic products overwhelms the world's ability to deal with them. Recent statistics showed that nearly 2.2 million tonnes of the plastic wastes were generated in ASEAN region alone (Greenpeace Southeast Asia, 2019). A recent study from Özsin and Pütün (2017), they mentioned that plastic waste such as high-density polyethylene (HDPE) is a potential source to be used for energy generation while eliminating them from the environment. For instance, kinetic analysis for thermal cracking of HDPE through isoconversional methods were conducted. The average activation energy (E_a) of HDPE (80 kJ/mol) obtained was significantly lower as compared to biomass such as rice hull (176.6 kJ/mol) and microalgae *Dunaliella tertiolecta* (145.7 kJ/mol) (Gan et al., 2018; Khedri & Elyasi, 2016; Shuping, Yulong, Mingde, Chun, & Junmao, 2010).

Co-pyrolysis is a process that involves the degradation of a mixture of two or more materials as feedstocks, in which a synergistic effect between materials can be induced that will reduce the E_a of the whole system. Many studies have reported that the co-pyrolysis of two mixtures would improve the product yield and selectivity without any new system configuration or addition of co-solvent into the system. For instance, Tang, Chen, Chen, Yang, and Chen (2019) conducted an investigation to improve pyrolytic oil quality extracted from microalgae by performing co-pyrolysis of microalgae *Nannochloropsis sp.* with low-density polyethylene

(LDPE) as feedstock. Notably, the addition of LDPE into the mixture has induced the increment of aliphatic hydrocarbon content of the pyrolytic oil from 22wt% to 77wt%. Another similar catalytic co-pyrolysis study was published by Garba et al. (2018). They pyrolyzed wood fuel and LDPE/HDPE mixture with catalyst zeolite ZSM-5 and the kinetics of non-catalytic and catalytic co-pyrolysis were compared. It was found that the addition of a catalyst promoted the thermal degradation of wood fuel by making it more reactive. The E_a of the non-catalytic pyrolysis of wood fuel/LDPE and wood fuel/HDPE were 54.0 and 95.9 kJ/mol, respectively. Meanwhile, the addition of ZSM-5 reduced the E_a values to 24.1 and 50.5 kJ/mol. The E_a of catalytic reaction was significantly lower than that of non-catalytic reaction. In short, it was concluded by the researchers that this catalytic co-pyrolysis of biomass with plastic showed good kinetic performance and can be an excellent thermochemical conversion method.

Recently, research showed powerful and high accuracy performance of the Artificial Neural Network (ANN) model on TGA weight loss data prediction. ANN is a human brain-inspired machine learning tool that are used to determine complex and numerous relationships. ANN is normally trained to recognize the data patterns in a short period of time by randomly selecting the weights from the input data. ANN model is also utilized to study and compare the differences of the kinetic and thermodynamic data obtained from experimental and ANN results. These outputs are substituted to chosen kinetic models and the kinetic parameters E_a and A will be determined by utilizing the data acquired from the iso-conversional kinetic models. Currently, the ANN approach was applied on waste pyrolysis studies of peanut shell, microalgae ash, high-ash sewage sludge, HDPE and LDPE (Al-Yaari & Dubdub, 2020; Bong et al., 2020; Dubdub & Al-Yaari, 2020; Naqvi et al., 2018). Furthermore, in 2021, Siddiqi et al., (2021) has reported that an empirical reaction model could well-translate the experimental

results across different heating rate. Such model aims to propose a generalized equation that can be applied in a range of different of heating rate in a pyrolysis system, predicting the degradation rate precisely without further experimental analysis.

Herein, a framework which targets to elucidate the synergistic effect of co-pyrolysis and the catalytic activity in thermal degradation of microalgae (*C. vulgaris)* and plastic waste (HDPE) binary mixtures by incorporating the domain of experiments, artificial intelligent, and empirical modelling has been proposed. Firstly, the experimental TGA data and ANN predicted results under different heating rates ranging from 10 K/min to 100 K/min were used to compute the kinetic and thermodynamic parameters through several iso-conversional kinetic models such as Friedman (FR), Kissinger Akahira Sunose (KAS), and Flynn-Wall-Ozawa (FWO). These kinetic and thermodynamic parameters including activation energy (E_a), pre-exponential value (A), enthalpy change (ΔH), entropy change (ΔS), and Gibb's free energy (ΔG). Thereupon identifying the most least error kinetic model and the best catalyst in co-pyrolysis thermal degradation, an empirical reaction model was developed for the whole system with the aid of multi-objective genetic algorithm (*GA*).

2.0 Materials and Methods

The research framework of this case study was shown **Fig. 1**, as follow: 1) Conducting thermal degradation experiments "8 different samples consisting *C. vulgaris* and plastic HDPE samples" via TGA; 2) Fitting the TGA results into different kinetic models (i.e. KAS, FWO, and Friedman); 3) Incorporating the *TT* and *LL* function of ANN modal to determine the regression of each modal; 4) Evaluating of kinetic and thermodynamic parameters using the models proposed; 5) Determining of the most precise iso-conversional kinetic models

based on the regression 6) Comparing the most precise iso-conventional modal with ANN predicted values in terms of kinetic parameters; and lastly 6) Developing an empirical model for the system via multi-objective genetic algorithm.

2.1 Sample preparation and experimental setup

The two main feedstock involved were *C. vulgaris* (Pure M) and plastic HDPE (Pure HDPE). The Pure M was obtained from Dr. Lam Man Kee, Centre for Biofuel and Biochemical, Universiti Teknologi PETRONAS (UTP), Malaysia while the Pure HDPE was provided by Shen Foong Plastic Industries Sdn. Bhd., Malaysia. The Pure M was dried for at least 24 hours at a temperature of 373 K to remove excess moisture and then, were grinded and sieved to a specific particle size of less than 750 µm, respectively. Thereafter, both samples were stored in an airtight container under room temperature. The samples of Pure M and Pure HDPE were mixed homogeneously in a weight ratio of 0.8:0.2 for the preparation of M/HDPE mixture. Meanwhile, the samples and catalysts preparation methods (e.g. size, weight ratio, loading) was based on previous study (Adler, 2020; Bong et al., 2020; Liew et al., 2021). Similarly, the co-pyrolysis studies for both the non-catalytic and catalytic co-pyrolysis experiments were conducted by using a thermogravimetric analyser (TGA) EXSTAR TG/DTG 6300 (Seiko Instrument Inc.). Each experimental runs are repeated thrice in order to obtain reproducible results. All the catalyst preparation and experimental procedures can be found in the **supplementary material.**

2.2 Artificial Neural Network (ANN) topology

A multiple layer perceptron ANN which consists of input layer, output layer and at least one hidden layer was used in this research. A transfer function relates both the input and output in a mathematical representation was preferred as larger range of output can be considered

(Dorofki et al., 2012).. The feedforward Levenberg-Marquardt (LM) back-propagation algorithm was used in modelling the ANN by using the MATLAB® 2019b software. Heating rate *(K/min)* unit and temperature *(K)* were the two main inputs obtained from the experimental TGA data. The inputs were sent to the two-layered neural network with different combinations of transfer functions for the prediction of weight loss of samples *(wt %)* output. The two transfer function combinations used in this research were tansig-tansig (*TT*) and logsig-logsig (*LL*) as both of these combinations were proven to generate higher accuracy outcome (>0.99) as reported in literature (Bong et al., 2020; Dubdub & Al-Yaari, 2020). The data sets were randomly split into three portions as follows: 70% training data, 15% validation data and 15% testing data by using the data division function '*dividerand*'. Number of neurons in the hidden layer ranging from 2 to 12 were used to model the network for the determination of average mean square error (MSE) after repeated simulation for at least 10 times. The number of neurons in the hidden layer that generated the lowest MSE were used for the following analysis. Then, the final set of ANN predicted output for different feedstocks and heating rates were determined based on the MSE value and regression value (R^2). Predicted data with low MSE and high R^2 is desirable as it signifies a smaller error and higher accuracy of the predicted data as compared to the experimental data. Then, TG curves of experimental and ANN predicted data were plotted. Kinetic and thermodynamic parameters of both experimental and ANN predicted data were computed and studied. The parameters and schematic of the ANN model developed in this research were tabulated and attached in **supplementary material**.

The ANN model developed was then used for model overfitting study to determine the optimum number of neurons in the hidden layer needed to prevent dataset overfit. The M/HDPE/Bifunctional HZSM-5/LS sample's dataset was trained in the ANN model and the

average MSE value of each neuron number combination was recorded. The changes of average MSE value was insignificant and negligible starting from neuron number 5. Simulation results such as the regression plots, kinetic and thermodynamic parameters were compared and the optimum number of neurons in the hidden layer were selected.

2.3 Kinetic analysis

Kinetic parameters such as activation energy, pre-exponential factor, and order of reaction are important as they can be related to the composition of the final products from catalytic co-pyrolysis, reactor scale-up and process optimization involved for this process. The kinetic analysis was modelled using an integrated one-step global isothermal process (**see supplementary material)**

2.3.1 Iso-conversional method

Iso-conversional models are less uncertain and more accurate for reaction mechanism of a non-linear investigation as compared to model-fitting methods (Vyazovkin & Sbirrazzuoli, 2006). Thus, in this study, the iso-conversional kinetic methods chosen were the KAS (integral), FWO (integral), FR (differential) methods. The kinetic parameters were computed by substituting the experimental and ANN predicted data into these iso-conversional equations and plotting linear plots.

2.3.1.1 Friedman (FR)

FR method has a higher probability to experience errors in estimating the E_a values due to its higher sensitivity towards data noise. The main FR equation is shown in Eq. (1).

$$ln\left(\beta\frac{d\alpha}{dt}\right) = ln\left(\frac{d\alpha}{dt}\right) = ln[A \cdot g(\alpha)] - \frac{E_a}{RT_\alpha} \quad \textbf{(1)}$$

The value of E_a is determined based on the gradient of a plot of $ln\left(\beta\frac{d\alpha}{dt}\right)$ *vs* $\frac{1}{T_\alpha}$. Then, the value of A is obtained from the y-intercept of the plot, $\ln[A \cdot g(\alpha)]$ by taking $n = 1$.

2.3.1.2 Kissinger-Akahira-Sunose (KAS)

KAS method has lower sensitivity towards data noise as compared to FR method and has lower chance of errors when estimating kinetic parameters. The KAS plot is plotted based on the equation shown in Eq. (2) below, in which the symbol T_α is known as the maximum reaction rate temperature.

$$ln\left(\frac{\beta}{T_\alpha^2}\right) = ln\left[\frac{RA}{E_a g(\alpha)}\right] - \frac{E_a}{RT_\alpha} \quad \textbf{(2)}$$

Based on the Eq. (2), the plot of $ln\left(\frac{\beta}{T_\alpha^2}\right)$ *vs* $\frac{1}{T_\alpha}$ is plotted. The term $-\frac{E_a}{R}$ *and* $ln\left[\frac{RA}{E_a g(\alpha)}\right]$ are the gradient and *y*-intercept respectively. Kinetic parameters E_a and *A* are determined.

2.3.1.3 Flynn-Wall-Ozawa (FWO)

FWO is an integral iso-conversional method that has lower sensitivity towards data noise and lower chance of errors in kinetic parameters estimation, same as KAS. However, a larger range of α is covered even for the cases in which the n value is not assumed. It also has lower accuracy than the KAS method. The FWO equation is shown in Eq. (3).

$$ln\,\beta = ln\left[\frac{E_a A}{Rg(\alpha)}\right] - 5.331 - 1.052\frac{E_a}{RT_\alpha} \quad \textbf{(3)}$$

From Eq. (3), $-1.052\frac{E_a}{RT_\alpha}$ is the gradient which the E_a is calculated whereas the value A is computed based on the y-intercept.

2.4 Thermodynamic analysis

In the thermodynamic study, the thermodynamic parameters were obtained by utilizing the kinetic parameters acquired from kinetic study. The parameters include enthalpy change (ΔH), entropy change (ΔS) and Gibb's free energy (ΔG). The equations to determine these parameters are expressed below (Xu & Chen, 2013):

$$\Delta H = E_a - RT \quad \textbf{(4)}$$

$$\Delta G = E_a + R \cdot T_m \cdot ln\left(\frac{K_B \cdot T_m}{h \cdot A}\right) \quad \textbf{(5)}$$

$$\Delta S = \frac{\Delta H - \Delta G}{T_m} \quad \textbf{(6)}$$

where K_B is known as the Boltzmann constant and the value is defined as 1.38×10^{-23} J/K. Then, h is referred to the Planck's constant and its value is 6.626×10^{-34} Js, T_m is referred to be the average DTG peak temperature in *K*.

2.5 Empirical Modelling

Empirical model-fitting method is often used for approximating the generalized function of model f *(α)* which considers all the probable mechanistic kinetics in the system. The Sestak and Berggren's (SB) model is a non-linear square fitting model that is widely used for best fitting model parameters computation (Ali & Bahadar, 2019). However, in our study, we have developed a series of modified the SB models instead of using the original SB model. This is because our degradation system consisted of a tri-solid mixture of M, HDPE and bifunctional catalyst, which is different from the literature. The three dependent terms of the model represent order (*n*), accelerating of degradation (*m*) and nucleation & diffusion-control mechanism (*p*), respectively shown in Eq. (7) (the most suitable model).

$$f(a) = (1-\alpha)^n \,.\, \alpha^m.\ p\left[\alpha^{\frac{(p-1)}{p}}\right].\ \frac{3}{2}[(1-\alpha)^{-\frac{1}{3}} - 1]^{-1} \quad \textbf{(7)}$$

where *n, m* and *p* are the unknown parameters corresponding to each mechanism. These unknown parameters can be computed through a generalized reduced gradient (GRG) algorithm and Eq. (8) is transformed in terms of the differential curve with respect to temperature as shown below:

$$\frac{da}{dt} = A_a e^{\left(\frac{-E_a}{RT_a}\right)} \times (1-\alpha)^n \,.\, \alpha^m.\ p\left[\alpha^{\frac{(p-1)}{p}}\right].\ \frac{3}{2}[(1-\alpha)^{-\frac{1}{3}} - 1]^{-1} \quad \textbf{(8)}$$

Apart from the aforementioned empirical reaction model proposed by Siddiqi et al., (2021), a further exploration on self-developed empirical model is in-trial. The empirical parameters (i.e., *n, m, p* from Eq.8) were found by minimizing the mean absolute percentage error (MAPE) of each empirical model Eq. (9) with the aid of multi-objective genetic algorithm in MATLAB® 2019b; the A_a, E_a and T_a values were pivoted in an averaged heating rate supplied in this study. Such empirical model parameter was bounded in the range of -100 to

100 for an effective search exploration for the minimal MAPE of the empirical model, in which a list of empirical models were compared with each other to identify the best empirical reaction model with the least MAPE.

$$\min MAPE = \frac{1}{N}\sum_{i=1}^{N}\left|\frac{\frac{d\alpha}{dt}_i^{exp} - \frac{d\alpha}{dt}_i^{model}}{\frac{d\alpha}{dt}_i^{exp}}\right| \times 100\% \quad \textbf{(9)}$$

3.0 Results and Discussion

3.1 Thermal degradation behaviour of pure samples

As observed from the DTG curve of Pure M **(see supplementary material)**, the whole thermal decomposition process can be classified into three different zones. The first zone or also known as the drying zone where the vaporization of moisture was observed to take place with some low volatile components. It was observed to begin from the room temperature 300 – 430 K. According to the study by Bach and Chen (2017), this zone happened due to the removal of moisture in the Pure M cells through vaporization and the water bounded by the cell surface tension. The second zone is the active pyrolysis zone where major weight loss of Pure M was observed from temperature 430 – 800 K. The cellulose and hemicellulose in Pure M started to decompose in this zone which contributes to the highest percentage of weight loss (Naqvi et al., 2019). The decomposition of the organic substances in Pure M such as carbohydrates, lipids and protein took placed. The formation of carbon monoxide (CO), carbon dioxide (CO_2), and other carbonaceous gases were observed at high pyrolysis temperature due to the vaporization of some non-volatile carbon compounds. Then, the passive zone (third zone) occurred between the temperature of 800 K and 1200 K where the carbonaceous materials such as tar and char decomposed. The long trailing curve was due to the slow decomposition rate of the lignin component in Pure M.

On the other hand, only one decomposition stage was clearly identified from the DTG curve of Pure HDPE as compared to Pure M. The Pure HDPE started to thermally decompose from 517 – 572 K. The degradation reached its final stage from temperature around 742 – 846 K. The Pure HDPE had a less complicated chemical structure as compared to that of Pure M, leading to a to the a lower degradation temperature. Therefore, a higher thermal decomposition rate was obtained in Pure HDPE as compared to Pure M shown in **Table 1.** In addition, a significant lower thermal decomposition rates were noticed when catalysts were introduced to the binary mixture. For instance, the DTG peak of non-catalytic Pure HDPE at HR10 was 23.06 wt%/min, while the catalytic co-pyrolysis of M-HDPE with HZSM-5, LS and Bifunctional HZSM-5/LS were 4.15 wt%/min, 5.07 wt%/min and 6.26 wt%/min, respectively.

3.2 Artificial Neural Network (ANN) Model

The ANN model in this study was trained for at least 10 times to obtain the average MSE for each transfer function combination and feedstock combination with increasing neuron number from 2 – 12; since the complexity of the thermal decomposition zones of catalytic co-pyrolysis may lead to non-convergence error of the model if one hidden layer and 1 neuron number are not being avoided. Notably, the two transfer function combinations of tansig-tansig (*TT*) and logsig-logsig (*LL*) have proven a higher accuracy outcome (>0.998) in the research. The lowest average MSE for *TT* and *LL* were 5.26×10^{-5} and 7.47×10^{-5}, respectively and were achieved at 12 number of neurons in the hidden layer. The achieved average MSE values were smaller than the values obtained by Bong et al. (2020), indicating that the simulation results in this study have smaller error and are highly comparable with

literature results. Thus, 12 number of neurons in the hidden layer were chosen for Pure M ANN model development and optimization which was used for TGA results generation in Section 3.3. The same ANN model development and optimization procedure was repeated for the remaining samples.

Fig. 2 shows the performance validation plots, error histograms and regressions plots obtained from neural network training of Pure M at HR10 for *TT* and *LL*. **Fig. 2(a)** indicates the ANN model performance (MSE) during the training, validation and test stages at epoch 1000 for both *TT* and *LL*. Besides that, the error histograms in **Fig. 2(b)** can be used to validate the model's accuracy. The errors achieved in both of the error histograms were within the acceptable range of ±1 (Çepelioğullar & Pütün, 2013). The regression plots in **Fig. 2(c)** shows that the R^2 achieved by all stages were exactly 1. These findings had further proven the reliability and accuracy of the ANN model to be used in the estimation of TGA results of complex biomass and plastic catalytic co-pyrolysis processes. TGA results and TG curves were generated upon every set of ANN model training on all eight samples at heating rates of HR10, HR20, HR30, HR50 and HR100.

3.3 Comparison between the experimental and ANN model

3.3.1 Thermal Degradation

The experimental results were analysed using the ANN models of *TT* and *LL* transfer functions. TG curves were plotted by taking weight loss of biomass and plastic feedstock as a function of temperature. The TG curves that compare the experimental and ANN models with *TT* and *LL* transfer functions at each heating rate are shown in **Fig. 3 and Table 2.**

From **Fig. 3 (a-e)**, the TG curves show high accuracy results where the weight loss data generated by both *TT* and *LL* transfer functions through ANN model agree closely with the experimental weight loss data. The reliability and accuracy of the ANN model developed with *TT* and *LL* transfer functions were further validated by the closely overlapped data between experimental and ANN generated results. For instance, according to the TG curve of experimental, *TT* and *LL* for M-HDPE/HZSM-5**,** the drying zone of the sample was observed from around 300 – 500 K. Then, the active decomposition zone occurred at 500 – 900 K where the organic structures of M and HDPE started to decompose. Third peak was observed at the passive zone from 900 K onward which signified the decomposition of other carbonaceous matter such as char, ash and tar. The TG curves of other samples can be broken down with the same concept. In addition, the TG curves of Pure M, Pure HDPE, M-HDPE/HZSM-5, M-HDPE/LS and M-HDPE/Bifunctional HZSM-5/LS tend to shift towards the right and upward side with increasing heating rates.

3.3.2 Kinetic and Thermodynamic Analyses

FR, FWO, and KAS models to determine the kinetic parameters of the non-catalytic and catalytic reactions. The thermal decomposition of the biomass and plastic were assumed as first order reactions where n=1. Later, Arrhenius plots of three models were plotted as shown in **Fig. 4** based on the experimental, *TT* and *LL* TGA results of M-HDPE/HZSM-5. The plots covered the conversions (α) from 0.1 – 0.9 with an interval of 0.1. The linear regression line data such as slope, y-intercept and R^2 were obtained from the best fit lines on the plots which can be used to determine the kinetic parameters and validate the accuracy of the kinetic

models. Apart from that, the R^2 values obtained from each best fit line on the Arrhenius plots (Experimental, *TT* and *LL*) are detailed in **Table 3.**

Based on **Table 3,** the overall average R^2 values for each model was recorded for comparison. As a result, the FWO model was observed to have higher overall average R^2 as compared to FR and KAS. The overall average R^2 values for FWO-*EXP*, FWO-*TT* and FWO-*LL* were 0.8901, 0.8865, and 0.8925, respectively. In addition, the analysis shows that the overall average R^2 values of *EXP* and *LL* were higher than *TT*. This further proves the high accuracy of *EXP* and *LL* data with these three iso-conversional kinetic models. The *EXP* data and *LL* data generated from the ANN model were more closely fitted to the best fit lines on Arrhenius plots. Thus, *EXP* and *LL* data were used for further kinetic and thermodynamic analysis from this point onwards to maintain the high accuracy results.

Table 4 presents the calculated E_a values of *EXP* and *LL* along with the percentage error (%) for comparison purposes. The calculated E_a from the kinetic models for Pure M and Pure HDPE were in the range from 201.83 – 498.99 kJ/mol and 140.33 – 289.62 kJ/mol, respectively. The non-catalytic E_a for Pure M recorded in Fong et al. (2019) was in the range of 156.16 – 158.10 kJ/mol which is slightly lower than present study. This would be due to the different kinetic models used in predicting the kinetic parameters. However, the E_a for Pure M is comparable with the E_a range of the same species of microalgae obtained from the literature by Vuppaladadiyam, Zhao, Memon, and Soomro (2019). It ranged from 184.06 – 390.31 kJ/mol and 182.53 – 382.14 kJ/mol for FR and KAS kinetic models, respectively. Similar study by Dubdub and Al-Yaari (2020) also highlighted that the pyrolysis of polyethylene waste that used the same three kinetic models were ranged from 185 – 206

kJ/mol. This shows that the E_a values calculated in this present study are in good agreement with literature findings.

Apart from that, the addition of catalysts for the catalytic co-pyrolysis of M and HDPE was one of the main highlights in this study. The calculated E_a values were observed to decrease drastically after the HZSM-5, LS and Bifunctional HZSM-5/LS were added as catalysts to the binary mixture of M and HDPE. The E_a range of M-HDPE/HZSM-5, M-HDPE/LS and M-HDPE/Bifunctional HZSM-5/LS for all three kinetic models were 87.53 – 146.80 kJ/mol, 95.87 – 163.91 kJ/mol and 67.26 – 103.02 kJ/mol respectively. The study by Fong et al. (2019) that used the same catalyst for similar feedstocks showed the similar catalytic activity and observation. Less than 100 kJ/mol of E_a were once achieved by the catalytic reaction. The chosen catalysts were able to shorten the reaction time and less energy was required for the thermal decomposition (Wang, Lei, Liu, & Bu, 2018). Based on the kinetic analysis, the lowest percentage error between E_a values of experimental and *LL* was observed from the FWO model as compared to FR and KAS models, especially for the catalytic feedstock such as M-HDPE/HZSM-5, M-HDPE/LS, and M-HDPE/Bifunctional HZSM-5/LS. Therefore, the most suitable kinetic model to be applied in this study was identified as the FWO model. Thermodynamic analysis of the catalytic feedstock was then conducted based on the kinetic parameters calculated from the FWO model.

Meanwhile, The average *A* range of M-HDPE/HZSM-5, M-HDPE/LS and M-HDPE/Bifunctional HZSM-5/LS for experimental and *LL* were $9.60 \times 10^8 - 1.04 \times 10^9\ s^{-1}$, $3.30 \times 10^{10} - 2.02 \times 10^{11}\ s^{-1}$, and $3.09 \times 10^7 - 4.44 \times 10^7\ s^{-1}$, respectively. The order of the *A* values was averagely maintained at $\geq 10^9$ for M-HDPE/HZSM-5 and M-

HDPE/LS which indicated no changes during the rotation of the active complex and reagent in the pyrolysis reaction (Xu & Chen, 2013). Thus, the catalytic co-pyrolysis of M-HDPE/HZSM-5 and M-HDPE/LS with higher *A* values were easier to react and thermally decomposed. The average Δ*H* of the M-HDPE/HZSM-5, M-HDPE/LS and M-HDPE/Bifunctional HZSM-5/LS were ranged from 88.62 – 91.53 kJ/mol, 96.70 – 102.52 kJ/mol, and 69.45 – 70.95 kJ/mol, respectively. Then, all the calculated Δ*G* values were positive and an increasing trend was observed from 0.1 – 0.9 conversion. The trend indicated that the energy of the system increased with increasing conversion (Bong et al., 2020). Lastly, all the Δ*S* were observed to be negative, ranging from -0.08 – -0.20 kJ/mol K for both experimental and *LL* data of all three catalytic feedstocks. Similar high negative Δ*S* values were also reported in previous literature studies (Bong et al., 2020; Fong et al., 2019; Xu & Chen, 2013). The high negative Δ*S* values also indicated a highly organized activated complex structure and can be characterized with "high degree of arrangement". When the feedstock is far from thermodynamic equilibrium, the Δ*S* will be higher which results in high reactivity and short reaction time.

Based on the kinetic and thermodynamic findings, the FWO model was chosen as the most suitable model as it gave the best prediction for kinetic and thermodynamic parameters with the least percentage error among the three kinetic models. Apart from that, the catalytic activity of the three catalysts were studied and compared. The E_a of the pure samples were reduced 62.5 % from average 200 kJ/mol to 75 kJ/mol with the presence of the Bifunctional HZSM-5/LS catalyst. This catalyst also provided the lowest average Δ*H* (69.45 kJ/mol) among the three catalysts which further proven that the Bifunctional HZSM-5/LS has a higher catalytic effect on M/HDPE as compared to LS and HZSM-5. A similar behaviour had been observed in the study conducted by Fong et al. (2020) utilising pure M in pyrolysis

process whereby the lowest E_a and ΔH values were achieved utilising the Bifunctional HZSM-5/LS catalyst. The presence of the catalyst enhances the secondary reaction in the pyrolysis process (Hu et al, 2011). It is also observed that the overall positive ΔH values achieved in this study indicate that the reaction is in endothermic whereby the heat was absorbed by the system in order for new bond to be formed.

3.4 ANN model fitting analysis

Based on the overfitting analysis, the differences between the average MSE values for neuron number from 5 – 12 were extremely minimal. This trend showed that the model has too much capacity which can learn it too well and overfit the training dataset. Thus, 5 number of neurons in the hidden layer were sufficient for the training of the datasets without overfitting the model which led to generalization error. A comparison of the simulation results in terms of regression plots, kinetic and thermodynamic parameters between the model with 5 and 12 number of neurons in the hidden layer **(see supplementary material).** The R^2 of neuron number 5 and 12 were 0.99996 and 0.99999, indicating the differences of the R^2 values between two simulation results were minimal and negligible. On the other hand, comparison in terms of kinetic and thermodynamic parameters with percentage errors are detailed in **Table 5**. Within expectation, the kinetic and thermodynamic parameters calculated for both sets of simulation results have high similarities associated with low average percentage errors.

3.5 Overall empirical reaction equation

A total of 12 different empirical reaction model were in-trial to identify the best model that could translate well the time-dependent derivative weight loss $\frac{d\alpha}{dt}$ of the M-

HDPE/Bifunctional HZSM-5/LS. MAPE of each empirical model proposed in this study is shown in **Table 6**, in which the least MAPE was found reported at 51.59%. The complete empirical model with the respective empirical parameter that resulted with least MAPE is shown (E.11), to be noted that the A_a, E_a, and T_a vary across the weight loss percentage α. The performance of such developed empirical reaction model **(Fig. 5)** was still in comparison with the experimental values reported alongside the empirical model proposed by Siddiqi et al. (2021) that reported with the (MAPE = 67.90%). Although the MAPE obtained was still less than <20%, suggesting a) the diffusion mechanism of tri-solid state of M, HDPE and catalysts is not fully covered; b) the heating rate being analysed is too large (100-100 K/min); 3) mixing of two materials which have large different composition. Nevertheless, to our best of our knowledge, this is the first empirical equation generated for tri-solid state degradation system with a considerable error. Future work on this research direction should be explored further with the aid of machine learning to develop a precise empirical equation for thermal degradation of materials.

$$\frac{d\alpha}{dt} = A_a e^{\left(\frac{-Ea}{RT_a}\right)} . (1-\alpha)^{22.18} . \alpha^{7.78} . \ 22.28 \left[\alpha^{\frac{(22.28-1)}{22.28}}\right] . \ \frac{3}{2}[(1-\alpha)^{-\frac{1}{3}} - 1]^{-1} \qquad \textbf{(E.11)}$$

4.0 Conclusion

With the aid of computational modelling (ANN and GA), a new empirical equation for the co-pyrolysis of the system (M-HDPE/ Bifunctional HZSM-5/LS) has been developed. From the *LL* transfer function-ANN model, the FWO model gave the best prediction for kinetic parameters with the highest R^2 values and lowest deviation achieved compared to other models. Notably, 5 number of neurons in the hidden layer were found to be sufficient for the data training without over-fit, suggesting that this method is suitable to be implemented in future research on TG data prediction. Among the three catalysts, the Bifunctional HZSM-

5/LS catalyst were able to shorten the reaction time and the E_a were reduced from range 144.93 – 225.84 kJ/mol to 75.37 – 76.90 kJ/mol. Lastly, the developed empirical equation can also be applied for other catalyst-material TG data prediction in future. For future research work, the incorporation of machine learning could be proposed to develop a precise empirical equation for thermal degradation of materials. Furthermore, the investigation of the yield and composition of the bioenergy produced from the co-pyrolysis of polyethylene and *C. vulgaris* would be a consideration to understand the synergistic effects of the blending of this mixture.

*E-supplementary data for this work can be found in e-version of this paper online

Acknowledgment

The authors would like to express their sincere gratitude to the Curtin University Malaysia and the Centre of Biofuel and Biochemical (CBBR) of Universiti Teknologi PETRONAS (UTP) for the technical support. Also, Loy, A.C.M would like to thank the Australian Government for providing financial (Research Training Program) support to this project.

References

[1] Adler, K. (2020). Europe emerges as leader in hydrogen economy. *IHS Markit*. Retrieved from https://ihsmarkit.com/research-analysis/europe-emerges-as-leader-in-hydrogen-economy.html.

[2] Al-Yaari, M., & Dubdub, I. J. (2020). Application of Artificial Neural Networks to Predict the Catalytic Pyrolysis of HDPE Using Non-Isothermal TGA Data. *Polymers, 12*, 1813. doi:10.3390/polym12081813.

[3] Alhazmi, H., & Loy, A. C. M. (2021). A review on environmental assessment of conversion of agriculture waste to bio-energy via different thermochemical routes:

Current and future trends. *Bioresource Technology Reports, 14*, 100682. doi:10.1016/j.biteb.2021.100682.

[4] Ali, I., & Bahadar, A. (2019). Thermogravimetric Characteristics and Non-isothermal Kinetics of Macro-Algae With an Emphasis on the Possible Partial Gasification at Higher Temperatures. *7*(7). doi:10.3389/fenrg.2019.00007.

[5] Bach, Q.-V., & Chen, W.-H. (2017). A comprehensive study on pyrolysis kinetics of microalgal biomass. *Energy Conversion and Management, 131*, 109-116.

[6] Bong, J. T., Loy, A. C. M., Chin, B. L. F., Lam, M. K., Tang, D. K. H., Lim, H. Y., . . . Yusup, S. (2020). Artificial neural network approach for co-pyrolysis of Chlorella vulgaris and peanut shell binary mixtures using microalgae ash catalyst. *Energy, 207*, 118289. doi:10.1016/j.energy.2020.118289.

[7] Çepelioğullar, Ö., & Pütün, A. E. (2013). Thermal and kinetic behaviors of biomass and plastic wastes in co-pyrolysis. *Energy Conversion and Management, 75*, 263-270. doi:10.1016/j.enconman.2013.06.036.

[8] Dorofki, M., Elshafie, A. H., Jaafar, O., Karim, O. A., Mastura, S. J. I. P. o. C., Biological, & Engineering, E. (2012). Comparison of artificial neural network transfer functions abilities to simulate extreme runoff data. *33*, 39-44.

[9] Dubdub, I., & Al-Yaari, M. (2020). Pyrolysis of Low Density Polyethylene: Kinetic Study Using TGA Data and ANN Prediction. *Polymers, 12*(4), 891. doi:10.3390/polym12040891.

[10] Fong, M. J. B., Loy, A. C. M., Chin, B. L. F., Lam, M. K., Yusup, S., & Jawad, Z. A. (2019). Catalytic pyrolysis of Chlorella vulgaris: Kinetic and thermodynamic analysis. *Bioresource Technology, 289*, 121689. doi:10.1016/j.biortech.2019.121689.

[11] Gan, D. K. W., Loy, A. C. M., Chin, B. L. F., Yusup, S., Unrean, P., Rianawati, E., & Acda, M. N. (2018). Kinetics and thermodynamic analysis in one-pot pyrolysis of rice hull using renewable calcium oxide based catalysts. *Bioresource Technology, 265*, 180-190. doi:10.1016/j.biortech.2018.06.003.

[12] Garba, M. U., Inalegwu, A., Musa, U., Aboje, A. A., Kovo, A. S., & Adeniyi, D. O. (2018). Thermogravimetric characteristic and kinetic of catalytic co-pyrolysis of biomass with low- and high-density polyethylenes. *Biomass Conversion and Biorefinery, 8*(1), 143-150. doi:10.1007/s13399-017-0261-y.

[13] Greenpeace Southeast Asia. (2019). *Policy Brief: Southeast Asia's struggle against the plastic waste trade*. Retrieved from https://storage.googleapis.com/planet4-philippines-stateless/2019/06/a72e63b1-waste-trade-report-5b-1.pdf?_ga=2.100347866.552988082.1560739055-281246604.1499670505.

[14] Hossain, M., Huda, A. S. N., Mekhilef, S., Seyedmahmoudian, M., Horan, B., Stojcevski, A., & Ahmed, M. (2018). A state-of-the-art review of hydropower in Malaysia as renewable energy: Current status and future prospects. *Energy Strategy Reviews, 22*, 426-437. doi:10.1016/j.esr.2018.11.001.

[15] International Energy Agency (IEA). (2019). *Renewables 2019*. Retrieved from IEA, Paris: https://www.iea.org/reports/renewables-2019.

[16] Jeong, G.-T., & Kim, S.-K. (2021). Statistical optimization of levulinic acid and formic acid production from lipid-extracted residue of Chlorella vulgaris. *Journal of Environmental Chemical Engineering, 9*(2), 105142. doi:10.1016/j.jece.2021.105142.

[17] Khedri, S., & Elyasi, S. (2016). Kinetic analysis for thermal cracking of HDPE: A new isoconversional approach. *Polymer Degradation and Stability, 129*, 306-318. doi:10.1016/j.polymdegradstab.2016.05.011.

[18] Hu, C., Yang, Y., Luo, J., Pan P., Tong, D., Li, G. (2010). Recent advances in the catalytic pyrolysis of biomass. *Frontiers of Chemical Science and Engineering*, *5*, 188-193. doi:10.1007/s11705-010-1015-6.

[19] Liew, J. X., Loy, A. C. M., Chin, B. L. F., AlNouss, A., Shahbaz, M., Al-Ansari, T., . . . Chai, Y. H. (2021). Synergistic effects of catalytic co-pyrolysis of corn cob and HDPE waste mixtures using weight average global process model. *Renewable Energy, 170*, 948-963. doi:10.1016/j.renene.2021.02.053.

[20] Monjed, M. K., Achour, B., Robson, G. D., & Pittman, J. K. (2021). Improved saccharification of Chlorella vulgaris biomass by fungal secreted enzymes for bioethanol production. *Algal Research, 58*, 102402. doi:10.1016/j.algal.2021.102402.

[21] Naqvi, S. R., Tariq, R., Hameed, Z., Ali, I., Naqvi, M., Chen, W.-H., . . . Taqvi, S. A. J. R. e. (2019). Pyrolysis of high ash sewage sludge: Kinetics and thermodynamic analysis using Coats-Redfern method. *131*, 854-860.

[22] Naqvi, S. R., Tariq, R., Hameed, Z., Ali, I., Taqvi, S. A., Naqvi, M., . . . Farooq, W. (2018). Pyrolysis of high-ash sewage sludge: Thermo-kinetic study using TGA and artificial neural networks. *Fuel, 233*, 529-538. doi:10.1016/j.fuel.2018.06.089.

[23] Özsin, G., & Pütün, A. E. (2017). Insights into pyrolysis and co-pyrolysis of biomass and polystyrene: Thermochemical behaviors, kinetics and evolved gas analysis. *Energy Conversion and Management, 149*, 675-685. doi:10.1016/j.enconman.2017.07.059.

[24] Shuping, Z., Yulong, W., Mingde, Y., Chun, L., & Junmao, T. (2010). Pyrolysis characteristics and kinetics of the marine microalgae Dunaliella tertiolecta using thermogravimetric analyzer. *Bioresource Technology, 101*(1), 359-365. doi:10.1016/j.biortech.2009.08.020.

[25] Tang, Z., Chen, W., Chen, Y., Yang, H., & Chen, H. (2019). Co-pyrolysis of microalgae and plastic: Characteristics and interaction effects. *Bioresource Technology, 274*, 145-152. doi:10.1016/j.biortech.2018.11.083.

[26] Vuppaladadiyam, A. K., Zhao, M., Memon, M. Z., & Soomro, A. F. (2019). Microalgae as a renewable fuel resource: a comparative study on the thermogravimetric and

kinetic behavior of four microalgae. *Sustainable Energy & Fuels, 3*(5), 1283-1296. doi:10.1039/C9SE00114J.

[27] Vyazovkin, S., & Sbirrazzuoli, N. (2006). Isoconversional Kinetic Analysis of Thermally Stimulated Processes in Polymers. *Macromolecular Rapid Communications, 27*(18), 1515-1532. doi:10.1002/marc.200600404.

[28] Wang, L., Lei, H., Liu, J., & Bu, Q. J. R. a. (2018). Thermal decomposition behavior and kinetics for pyrolysis and catalytic pyrolysis of Douglas fir. *RSC Advances 8*(4), 2196-2202. doi:10.1039/C7RA12187C.

[29] Xu, Y., & Chen, B. (2013). Investigation of thermodynamic parameters in the pyrolysis conversion of biomass and manure to biochars using thermogravimetric analysis. *Bioresource Technology, 146*, 485-493. doi:10.1016/j.biortech.2013.07.086.

CRediT authorship contribution statement

Tshun Li Yap – Original draft; Data Curation; Formal analysis; Investigation; Software.

Adrian Chun Minh Loy – Formal analysis; Writing – Review & editing; Investigation; Software.

Bridgid Lai Fui Chin – Formal analysis; Supervision; Writing – Review & editing; Investigation.

Juin Yau Lim – Formal analysis; Writing – Review & editing; Investigation; Software.

Hatem Alhamzi – Formal analysis; Writing – Review & editing.

Yee Ho Chai – Formal analysis; Writing – Review & editing.

Chung Loong Yiin – Formal analysis; Writing – Review & editing.

Kin Wai Cheah - Formal analysis; Writing - Review & editing.

Melvin Xin Jie Wee - Writing - Review & editing.

Man Kee Lam – Resources; Formal analysis; Writing – Review & editing.

Zeinab Abbas Jawad – Formal analysis; Writing – Review & editing.

Suzana Yusup - Resources; Formal analysis; Writing – Review & editing.

Serene Sow Mun Lock - Resources; Formal analysis; Writing – Review & editing.

Declaration of Competing Interest

☒ The authors declare that they have no known competing financial interests or personal relationships that could have appeared to influence the work reported in this paper.

☐The authors declare the following financial interests/personal relationships which may be considered as potential competing interests:

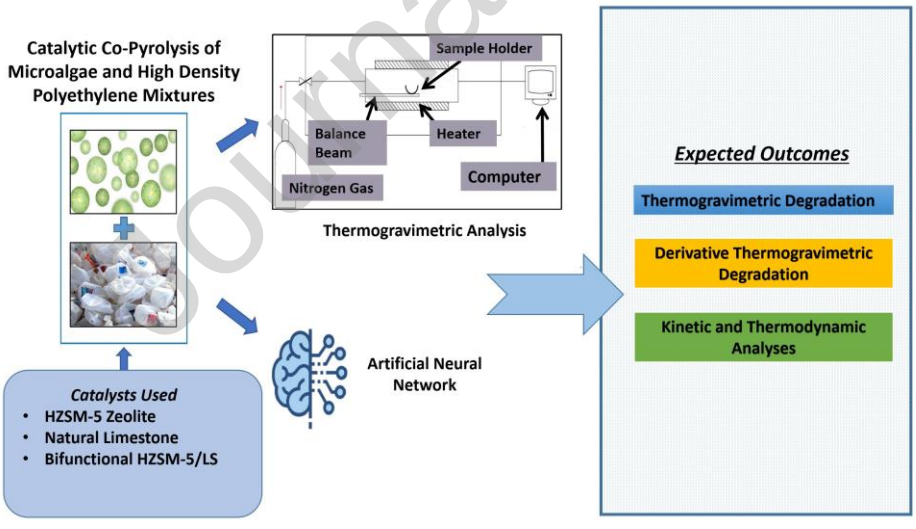

Graphical abstract

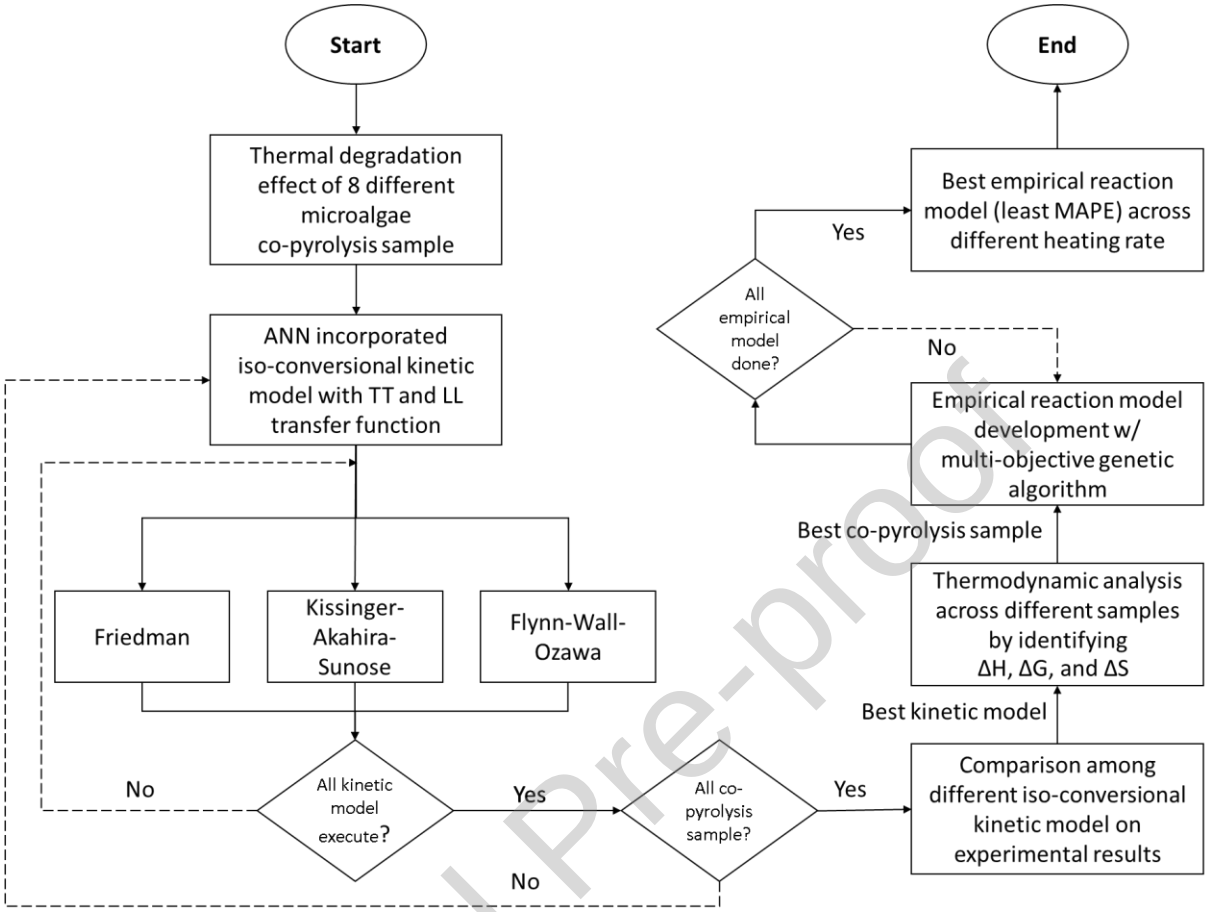

Fig. 1. Research framework proposed of co-pyrolysis of microalgae and plastic waste binary mixture.

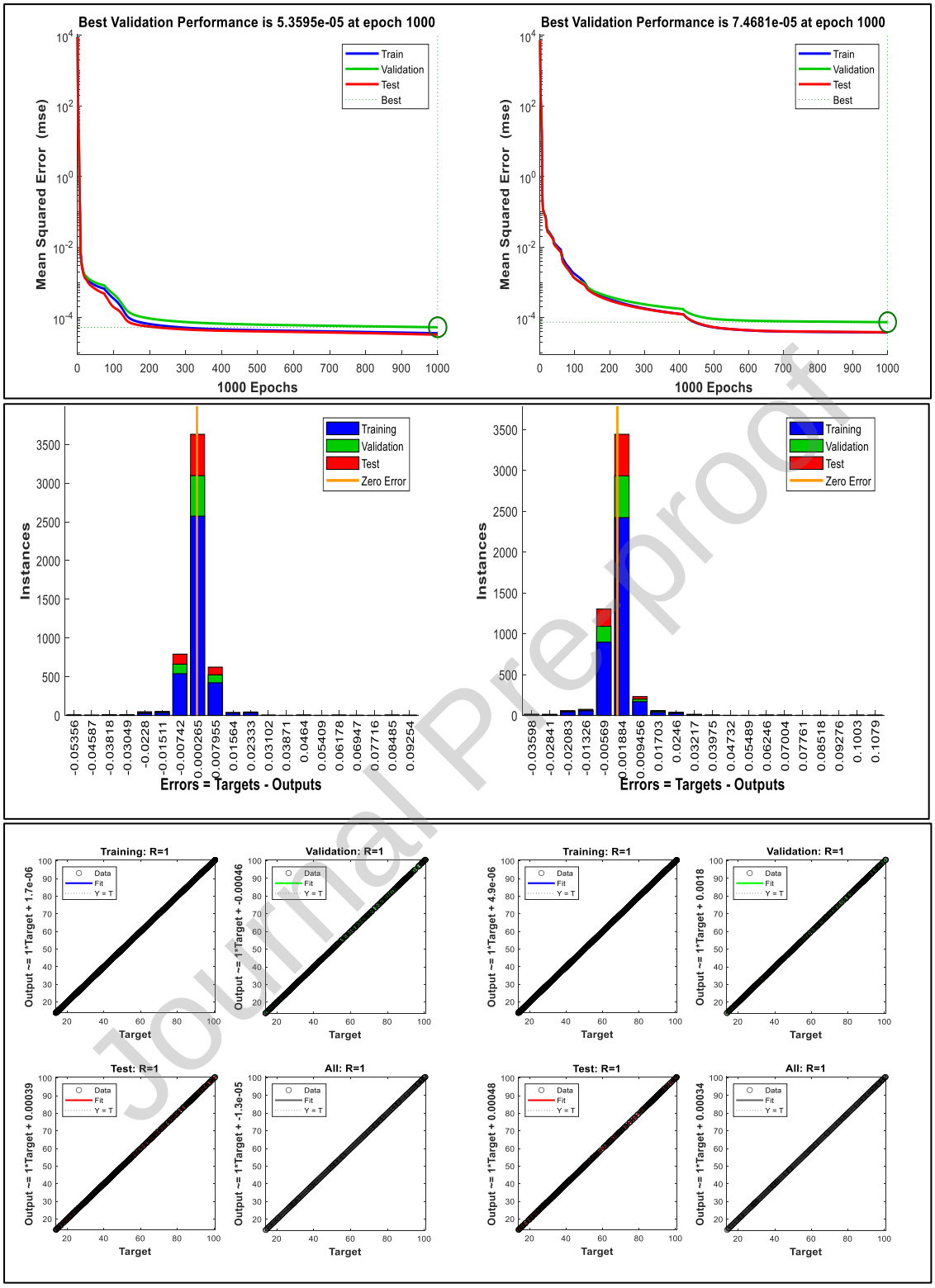

Fig. 2. (a) Performance validation plots, (b) Error histograms and (c) Regressions plots obtained from ANN training of Pure M at HR10 for *TT* and *LL*.

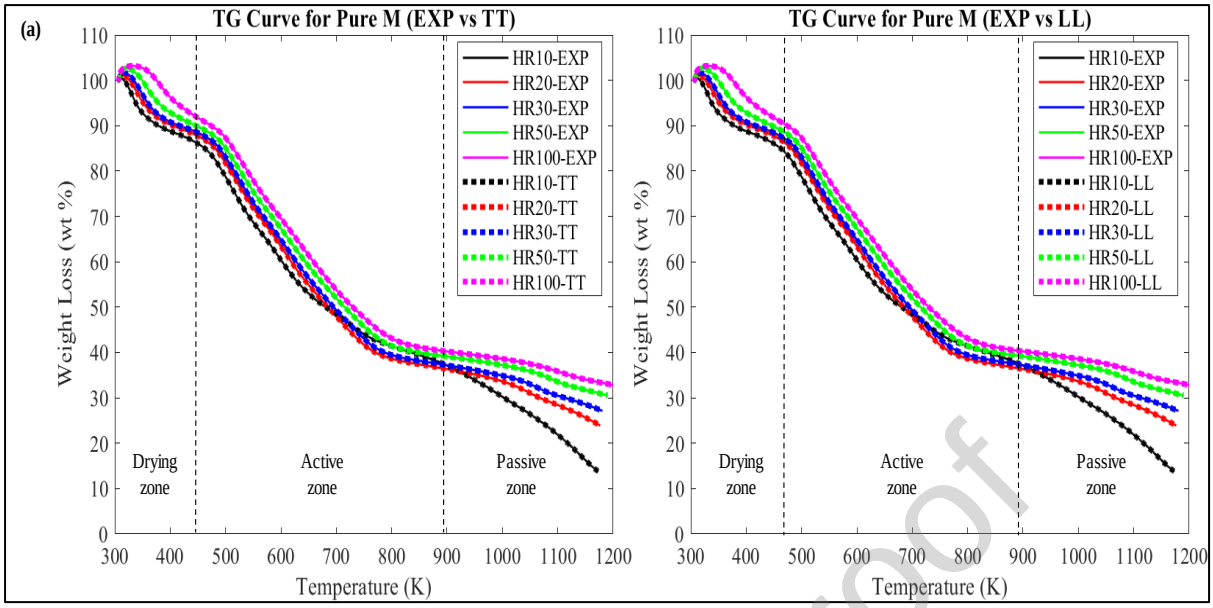

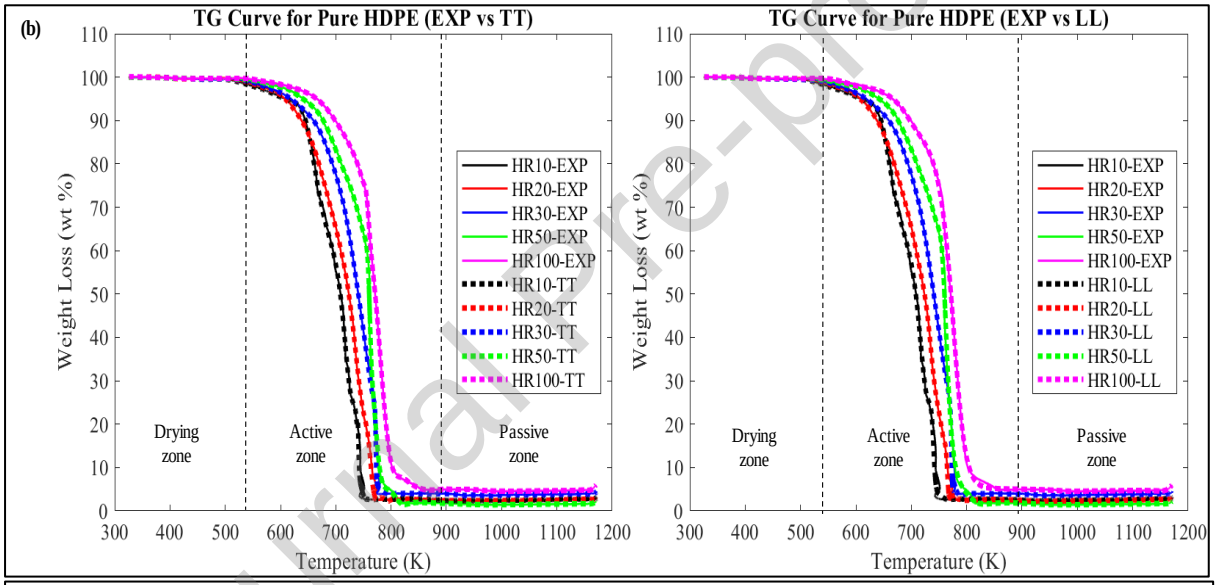

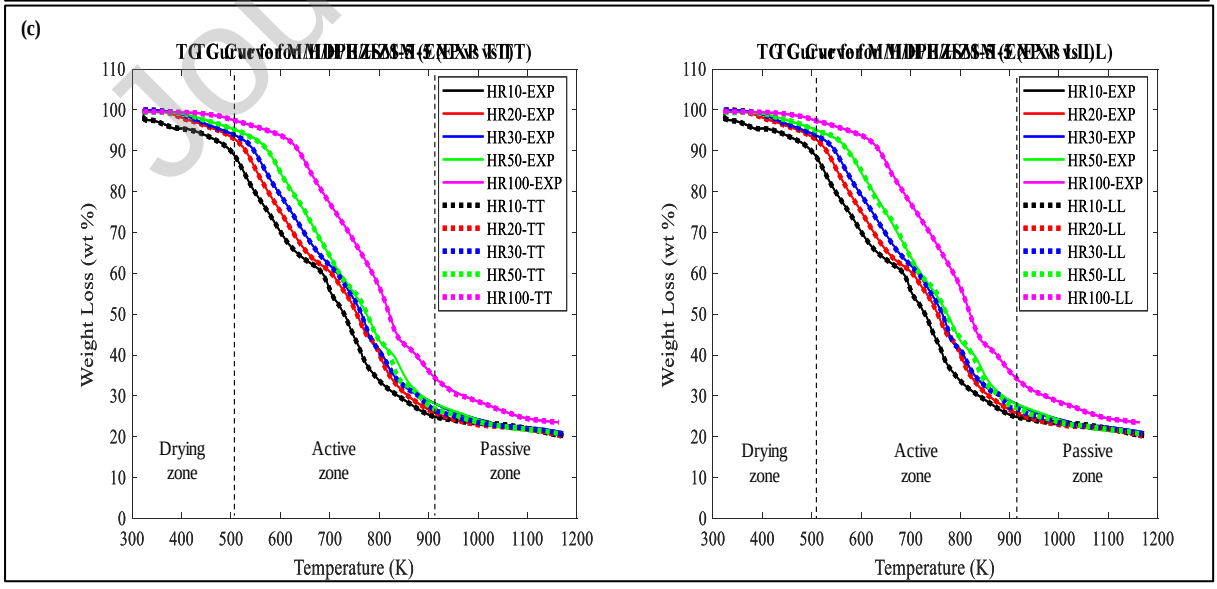

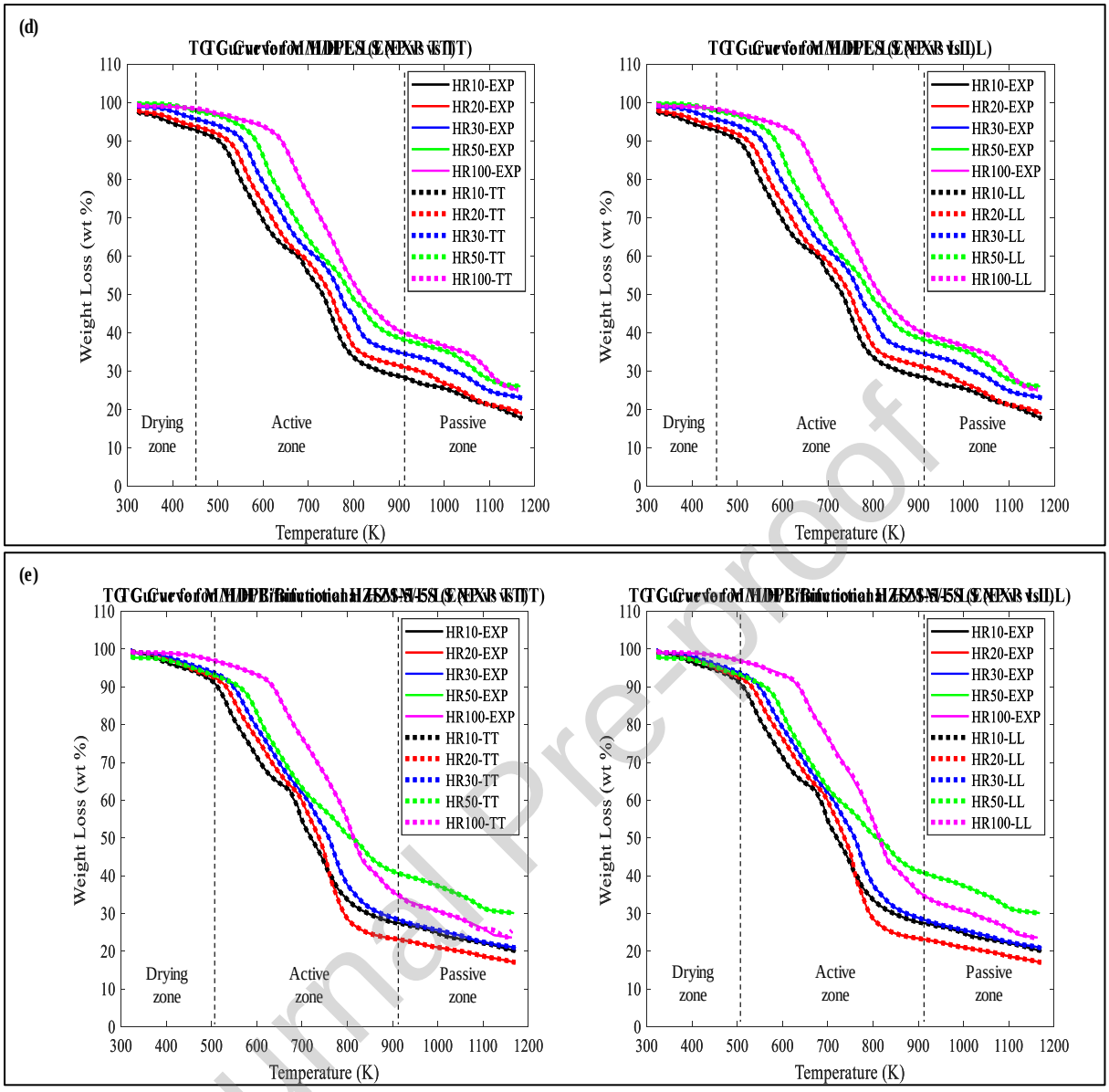

Fig. 3. Comparison between *EXP*, *TT* and *LL* TG curves of (a) Pure M, (b) Pure HDPE, (c) M/HDPE/HZSM-5, (d) M/HDPE/LS and (e) M/HDPE/Bifunctional HZSM-5/LS.

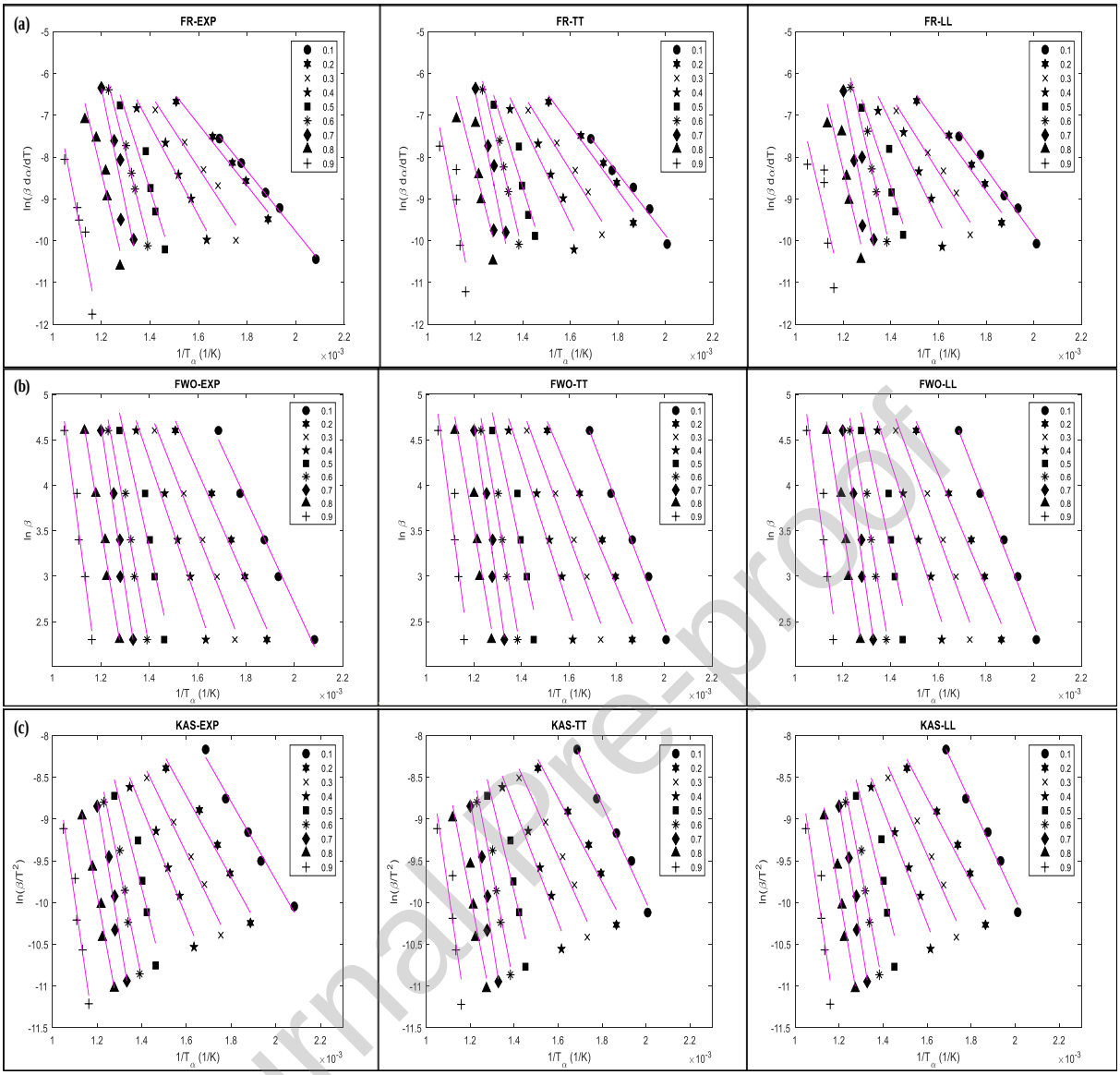

Fig. 4. Arrhenius plots of M/HDPE/HZSM-5 (*EXP*, *TT* and *LL*) for different kinetic models (a) FR, (b) FWO and (c) KAS.

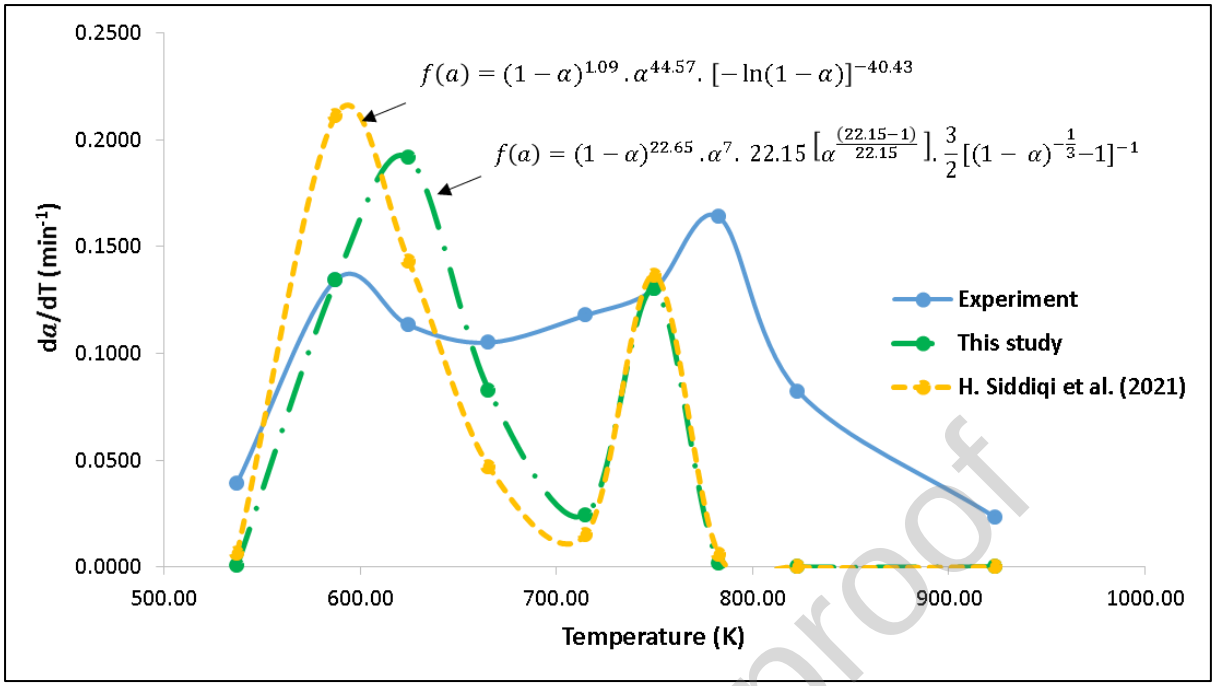

Fig. 5. Generalized empirical reaction model according to FWO kinetics across different weight loss range in an averaged heating rate.

Table 1. Active decomposition stage data of Pure M, Pure HDPE, M-HDPE/HZSM-5, M-HDPE/LS and M-HDPE/Bifunctional HZSM-5/LS.

Sample	β (K/min)	$T_{initial}$ (K)	T_{final} (K)	T_{peak} (K)	Remaining residue (wt%)	DTG_{peak} (wt%/min)
Pure M	HR10	420.66	866.67	519.96	38.76	2.16
	HR20	415.75	837.81	520.12	37.63	4.34
	HR30	417.88	838.38	519.64	38.40	6.39
	HR50	419.82	869.24	536.73	39.65	10.23
	HR100	455.55	906.42	520.41	40.14	21.11
Pure HDPE	HR10	626.31	743.56	740.64	3.21	23.06
	HR20	518.82	768.05	759.07	2.59	26.75
	HR30	516.94	774.55	773.53	3.92	64.06
	HR50	529.94	813.72	772.76	1.74	72.06

Sample	β (K/min)	$T_{initial}$ (K)	T_{final} (K)	T_{peak} (K)	Remaining residue (wt%)	DTG_{peak} (wt%/min)
	HR100	522.61	855.32	781.85	4.89	147.31
M-HDPE/HZSM-5	HR10	484.15	879.15	764.15	26.75	4.15
	HR20	481.15	899.15	797.15	26.74	8.29
	HR30	494.15	947.15	773.15	26.18	11.91
	HR50	508.15	983.15	783.15	24.91	13.31
	HR100	433.15	1123.15	813.15	24.01	35.94
M-HDPE/LS	HR10	509.15	796.15	754.15	34.13	5.07
	HR20	513.15	821.15	757.15	34.46	7.78
	HR30	521.15	857.15	800.15	36.41	9.19
	HR50	503.15	913.15	603.15	38.21	15.35
	HR100	533.15	933.15	663.15	39.06	27.39
M-HDPE/Bifunctional HZSM-5/LS	HR10	506.15	793.15	691.15	34.60	6.26
	HR20	511.15	837.15	757.15	25.34	13.08
	HR30	515.15	887.15	773.15	29.41	12.33
	HR50	523.15	913.15	598.15	40.64	13.27
	HR100	563.15	963.15	803.15	31.96	34.74

Table 2. R^2 values (Experimental (*EXP*), *TT* and *LL*) obtained from different feedstock combinations with different kinetic models (FR, FWO and KAS).

Kinetic model		FR			FWO			KAS		
Source	*α*	*EXP*	*TT*	*LL*	*EXP*	*TT*	*LL*	*EXP*	*TT*	*LL*
Pure M	0.1	0.9578	0.9598	0.9603	0.9753	0.9783	0.9783	0.9608	0.9678	0.9672
	0.2	0.9911	0.9968	0.9968	0.9893	0.9966	0.9966	0.9879	0.9962	0.9962
	0.3	0.9756	0.9868	0.9875	0.9786	0.9880	0.9880	0.9764	0.9870	0.9870
	0.4	0.9307	0.9283	0.9283	0.9356	0.9321	0.9321	0.9310	0.9277	0.9277
	0.5	0.9219	0.9973	0.9973	0.9222	0.9250	0.9165	0.9175	0.9214	0.9119
	0.6	0.7336	0.6612	0.6952	0.7478	0.6728	0.6949	0.7379	0.6622	0.6852
	0.7	0.0292	0.0441	0.0501	0.0286	0.0498	0.0571	0.0253	0.0547	0.0625
	0.8	0.5345	0.5928	0.5916	0.3746	0.4398	0.4390	0.4071	0.4722	0.4709
	0.9	0.9250	0.9501	0.9456	0.9920	0.9984	0.9961	0.9936	0.9988	0.9970
Average		**0.7777**	**0.7908**	**0.7947**	**0.7716**	**0.7756**	**0.7776**	**0.7708**	**0.7764**	**0.7784**
Pure HDPE	0.1	0.9464	0.9507	0.9489	0.8446	0.8383	0.8372	0.8185	0.8115	0.8102
	0.2	0.9801	0.9813	0.9837	0.9628	0.9685	0.9653	0.9541	0.9610	0.9567
	0.3	0.9602	0.9599	0.9571	0.9786	0.9777	0.9773	0.9732	0.9722	0.9718
	0.4	0.9344	0.9465	0.9859	0.9479	0.9491	0.9517	0.9368	0.9382	0.9416
	0.5	0.9684	0.9894	0.9873	0.9647	0.9711	0.9733	0.9583	0.9659	0.9685
	0.6	0.9855	0.9740	0.9796	0.9867	0.9822	0.9820	0.9847	0.9795	0.9792
	0.7	0.9796	0.9414	0.9509	0.9636	0.9698	0.9631	0.9583	0.9653	0.9576
	0.8	0.9838	0.9186	0.9678	0.9472	0.9349	0.9410	0.9405	0.9268	0.9337
	0.9	0.9762	0.5481	0.5471	0.9628	0.9752	0.9673	0.9585	0.9721	0.9632
Average		**0.9683**	**0.9122**	**0.9231**	**0.9510**	**0.9519**	**0.9509**	**0.9425**	**0.9436**	**0.9425**
M/HDPE/ HZSM-5	0.1	0.9970	0.9791	0.9843	0.9904	0.9924	0.9910	0.9872	0.9889	0.9867
	0.2	0.9831	0.9673	0.9736	0.9853	0.9777	0.9777	0.9749	0.9639	0.9639
	0.3	0.9483	0.9568	0.9611	0.9893	0.9772	0.9714	0.9822	0.9645	0.9560
	0.4	0.9722	0.9300	0.9174	0.9831	0.9669	0.9735	0.9738	0.9512	0.9607

Kinetic model		FR			FWO			KAS		
Source	α	*EXP*	*TT*	*LL*	*EXP*	*TT*	*LL*	*EXP*	*TT*	*LL*
	0.5	0.9241	0.9013	0.8626	0.9097	0.8894	0.8461	0.8845	0.8608	0.8082
	0.6	0.9892	0.9745	0.9591	0.9674	0.9642	0.9642	0.9591	0.9555	0.9555
	0.7	0.8715	0.8099	0.8307	0.9625	0.9519	0.9741	0.9551	0.9428	0.9690
	0.8	0.9210	0.7561	0.8540	0.9838	0.9293	0.9687	0.9799	0.9113	0.9614
	0.9	0.8981	0.7393	0.5968	0.9676	0.8655	0.8706	0.9608	0.8410	0.8466
Average		**0.9449**	**0.8905**	**0.8822**	**0.9710**	**0.9461**	**0.9486**	**0.9619**	**0.9311**	**0.9342**
M/HDPE/ LS	0.1	0.9662	0.9431	0.9453	0.9884	0.9717	0.9744	0.9790	0.9529	0.9570
	0.2	0.9414	0.9140	0.9247	0.9738	0.9601	0.9601	0.9581	0.9368	0.9368
	0.3	0.9566	0.9147	0.9120	0.9663	0.9388	0.9346	0.9496	0.9100	0.9039
	0.4	0.9150	0.9012	0.9095	0.9614	0.9443	0.9481	0.9439	0.9224	0.9273
	0.5	0.9171	0.9172	0.9080	0.8565	0.8313	0.8431	0.8264	0.7996	0.8136
	0.6	0.9929	0.9083	0.9872	0.9885	0.9887	0.9887	0.9865	0.9868	0.9868
	0.7	0.9327	0.9298	0.9727	0.9886	0.9878	0.9951	0.9862	0.9854	0.9940
	0.8	0.8220	0.8081	0.8431	0.9613	0.9524	0.9536	0.9490	0.9383	0.9395
	0.9	0.8784	0.7919	0.8191	0.8997	0.8618	0.8697	0.8813	0.8393	0.8481
Average		**0.9247**	**0.8920**	**0.9135**	**0.9538**	**0.9374**	**0.9408**	**0.9400**	**0.9191**	**0.9230**
M/HDPE/ Bifunctional HZSM-5/LS	0.1	0.7697	0.9160	0.9540	0.6848	0.9134	0.8948	0.5524	0.8688	0.8365
	0.2	0.9271	0.9102	0.9179	0.9455	0.9574	0.9600	0.9172	0.9353	0.9389
	0.3	0.7755	0.7746	0.8424	0.8665	0.8819	0.8893	0.8111	0.8341	0.8432
	0.4	0.7287	0.7387	0.6713	0.806	0.8287	0.8287	0.7386	0.7700	0.7700
	0.5	0.6624	0.7192	0.7267	0.6338	0.6746	0.6683	0.5520	0.6109	0.5952
	0.6	0.9951	0.9974	0.9869	0.9046	0.9328	0.9356	0.8827	0.9171	0.9205
	0.7	0.6953	0.5948	0.5693	0.9719	0.9542	0.9623	0.9650	0.9445	0.9532
	0.8	0.5941	0.5784	0.5068	0.8731	0.8560	0.8620	0.8360	0.818	0.8215
	0.9	0.5997	0.2892	0.5019	0.5693	0.3950	0.6021	0.4400	0.2645	0.4716

Kinetic model		FR			FWO			KAS		
Source	α	*EXP*	*TT*	*LL*	*EXP*	*TT*	*LL*	*EXP*	*TT*	*LL*
Average		**0.7497**	**0.7243**	**0.7419**	**0.8062**	**0.8216**	**0.8448**	**0.7439**	**0.7737**	**0.7945**
Overall Average		**0.8731**	**0.8420**	**0.8511**	**0.8901**	**0.8865**	**0.8925**	**0.8713**	**0.8688**	**0.8745**

Table 3. E_a values and percentage error between experimental and *LL* from different kinetic models: FR, FWO and KAS.

Kinetic model		FR			FWO			KAS		
Parameters	α	E_a (kJ/mol)		%Error	E_a (kJ/mol)		%Error	E_a (kJ/mol)		%Error
Source		*EXP*	*LL*		*EXP*	*LL*		*EXP*	*LL*	
Pure M	0.1	51.36	58.18	13.28	31.28	34.38	9.92	26.25	29.58	12.68
	0.2	293.10	331.85	13.22	129.82	150.44	15.89	128.34	150.08	16.94
	0.3	383.08	460.60	20.24	178.95	215.04	20.17	179.40	217.40	21.18
	0.4	551.65	600.04	8.77	251.09	275.52	9.73	254.66	280.37	10.10
	0.5	656.12	707.68	7.86	306.85	338.26	10.24	312.59	345.65	10.58
	0.6	910.02	1051.98	15.60	405.38	463.92	14.44	415.53	477.13	14.83
	0.7	425.83	476.15	11.82	186.35	227.33	21.99	184.30	250.89	36.13
	0.8	574.03	595.93	3.81	173.12	183.76	6.15	195.00	206.19	5.73
	0.9	222.28	208.52	6.19	153.62	143.93	6.31	178.24	167.99	5.75
Average		**451.94**	**498.99**	**11.20**	**201.83**	**225.84**	**12.76**	**208.26**	**236.14**	**14.88**
Pure HDPE	0.1	219.28	230.84	5.27	117.38	117.87	0.42	112.42	112.93	0.45
	0.2	179.68	182.68	1.67	106.90	102.96	3.69	100.88	96.72	4.13
	0.3	223.27	212.99	4.61	103.75	105.25	1.45	97.27	98.88	1.65
	0.4	240.92	231.52	3.90	117.74	119.50	1.50	111.77	113.61	1.65
	0.5	276.68	291.71	5.43	140.13	142.70	1.83	135.14	137.85	2.00
	0.6	331.70	335.02	1.00	161.20	156.92	2.65	157.20	152.70	2.86
	0.7	357.96	324.03	9.48	166.52	164.15	1.42	162.69	160.22	1.52

Kinetic model		FR			FWO			KAS		
Parameters	α	E_a (kJ/mol)		%Error	E_a (kJ/mol)		%Error	E_a (kJ/mol)		%Error
Source		*EXP*	*LL*		*EXP*	*LL*		*EXP*	*LL*	
	0.8	375.68	337.39	10.19	192.41	196.71	2.24	189.77	194.29	2.38
	0.9	401.37	228.80	42.99	209.45	198.25	5.35	207.55	195.80	5.66
Average		**289.62**	**263.89**	**9.39**	**146.16**	**144.93**	**2.28**	**141.63**	**140.33**	**2.48**
M-HDPE/HZSM-5	0.1	60.18	65.75	9.27	45.43	53.70	18.19	38.94	47.47	21.88
	0.2	61.11	65.53	7.23	47.92	49.29	2.87	40.55	41.94	3.44
	0.3	74.15	75.20	1.41	53.90	57.07	5.89	46.18	49.45	7.07
	0.4	90.60	97.37	7.47	62.74	64.87	3.40	54.79	56.97	3.99
	0.5	152.93	142.07	7.10	95.45	96.46	1.06	88.20	89.21	1.14
	0.6	193.28	203.47	5.27	116.19	121.19	4.31	109.50	114.72	4.78
	0.7	235.71	229.46	2.65	140.91	144.70	2.69	135.09	139.05	2.94
	0.8	202.98	197.58	2.66	127.37	132.85	4.30	120.17	125.91	4.77
	0.9	250.23	200.97	19.69	161.05	157.03	2.49	154.37	150.08	2.78
Average		**146.80**	**141.93**	**6.97**	**94.55**	**97.47**	**5.02**	**87.53**	**90.53**	**5.87**
M-HDPE/LS	0.1	49.23	58.69	19.21	35.93	43.59	21.32	28.76	36.46	26.80
	0.2	66.89	68.68	2.68	50.22	49.91	0.60	42.90	42.44	1.08
	0.3	83.09	80.82	2.74	58.71	58.28	0.73	51.28	50.66	1.20
	0.4	98.10	109.43	11.55	66.04	70.73	7.10	58.32	63.17	8.33
	0.5	195.37	193.92	0.74	110.17	119.54	8.51	103.84	113.64	9.44

Kinetic model		FR			FWO			KAS		
Parameters	α	E_a (kJ/mol)		%Error	E_a (kJ/mol)		%Error	E_a (kJ/mol)		%Error
Source		*EXP*	*LL*		*EXP*	*LL*		*EXP*	*LL*	
M-HDPE/Bifunctional HZSM-5/LS	0.6	252.97	253.91	0.37	165.23	176.97	7.11	161.18	173.50	7.64
	0.7	156.60	171.51	9.52	144.53	152.03	5.19	138.84	146.72	5.67
	0.8	123.50	128.39	3.97	107.60	110.15	2.37	99.01	101.66	2.68
	0.9	346.06	409.84	18.43	186.21	196.11	5.32	178.68	189.04	5.80
Average		**152.42**	**163.91**	**7.69**	**102.74**	**108.59**	**6.47**	**95.87**	**101.92**	**7.63**
	0.1	55.49	58.24	4.96	36.31	42.80	17.89	28.88	35.59	23.22
	0.2	67.50	73.42	8.78	52.02	53.35	2.55	44.75	46.14	3.10
	0.3	75.66	83.88	10.87	56.64	58.68	3.60	48.93	51.07	4.37
	0.4	94.47	88.36	6.47	62.99	66.00	4.77	54.92	58.06	5.72
	0.5	121.27	119.41	1.54	75.35	80.27	6.53	67.05	72.21	7.69
	0.6	177.04	182.77	3.24	112.93	115.80	2.54	106.21	109.23	2.84
	0.7	152.00	134.56	11.47	124.87	120.32	3.65	118.25	113.45	4.06
	0.8	105.06	95.30	9.29	94.13	92.51	1.73	85.25	83.53	2.02
	0.9	78.70	86.56	9.98	63.08	62.35	1.16	51.05	50.23	1.61
Average		**103.02**	**102.50**	**7.40**	**75.37**	**76.90**	**4.94**	**67.26**	**68.84**	**6.07**

3

Table 4. Pre-exponential factor (*A*) and thermodynamic parameters (*EXP vs LL*) of M-HDPE/HZSM-5, M-HDPE/LS and M-HDPE/Bifunctional HZSM-5/LS with FWO kinetic model.

Kinetic model		FWO							
Source		*EXP*				*LL*			
Parameters	α	A (s^{-1})	ΔH (kJ/mol)	ΔG (kJ/mol)	ΔS (kJ/mol.K)	A (s^{-1})	ΔH (kJ/mol)	ΔG (kJ/mol)	ΔS (kJ/mol.K)
M-HDPE/HZSM-5	0.1	5.84×10^{3}	40.97	187.62	-0.19	3.17×10^{4}	49.20	184.83	-0.17
	0.2	8.32×10^{3}	43.05	187.79	-0.18	1.04×10^{4}	44.41	187.68	-0.18
	0.3	2.00×10^{4}	48.69	188.03	-0.18	3.53×10^{4}	51.86	187.51	-0.17
	0.4	6.81×10^{4}	57.20	188.87	-0.17	9.43×10^{4}	59.31	188.88	-0.16
	0.5	7.56×10^{6}	89.46	190.80	-0.13	8.82×10^{6}	90.46	190.81	-0.13
	0.6	1.09×10^{8}	109.87	194.12	-0.11	2.30×10^{8}	114.86	194.21	-0.10
	0.7	3.08×10^{9}	134.35	196.98	-0.08	5.52×10^{9}	138.13	197.28	-0.08
	0.8	1.88×10^{8}	120.47	201.73	-0.10	4.24×10^{8}	125.95	201.88	-0.10
	0.9	5.26×10^{9}	153.56	213.63	-0.08	3.41×10^{9}	149.58	212.44	-0.08
Average		$\mathbf{9.60 \times 10^{8}}$	**88.62**	-	-	$\mathbf{1.04 \times 10^{9}}$	**91.53**	-	-
M-HDPE/LS	0.1	7.52×10^{2}	31.43	176.97	-0.20	2.82×10^{3}	38.97	176.77	-0.19
	0.2	1.25×10^{4}	45.33	174.53	-0.18	1.06×10^{4}	44.98	175.24	-0.18
	0.3	5.39×10^{4}	53.55	174.34	-0.17	4.53×10^{4}	53.08	174.95	-0.17
	0.4	1.37×10^{5}	60.55	176.12	-0.16	2.94×10^{5}	65.21	176.28	-0.16
	0.5	1.13×10^{8}	104.25	180.32	-0.11	4.93×10^{8}	113.60	180.92	-0.09
	0.6	2.85×10^{11}	158.92	188.78	-0.04	1.78×10^{12}	170.65	189.61	-0.03

Kinetic model		FWO							
Source		*EXP*				*LL*			
Parameters	α	A (s^{-1})	ΔH (kJ/mol)	ΔG (kJ/mol)	ΔS (kJ/mol.K)	A (s^{-1})	ΔH (kJ/mol)	ΔG (kJ/mol)	ΔS (kJ/mol.K)
	0.7	4.97×10^{9}	137.95	192.15	-0.08	1.48×10^{10}	145.43	193.16	-0.07
	0.8	8.57×10^{6}	100.59	193.08	-0.13	1.20×10^{7}	103.13	193.62	-0.13
	0.9	6.96×10^{9}	177.71	231.84	-0.08	2.12×10^{10}	187.59	235.10	-0.07
Average		$\mathbf{3.30 \times 10^{10}}$	**96.70**	-	-	$\mathbf{2.02 \times 10^{11}}$	**102.52**	-	-
M-HDPE/Bifunctional HZSM-5/LS	0.1	8.52×10^{2}	31.84	178.45	-0.20	2.67×10^{3}	38.23	178.08	-0.19
	0.2	1.79×10^{4}	47.14	175.82	-0.18	2.22×10^{4}	48.44	175.86	-0.18
	0.3	3.42×10^{4}	51.45	176.54	-0.17	4.77×10^{4}	53.47	176.58	-0.17
	0.4	7.24×10^{4}	57.46	178.39	-0.17	1.17×10^{5}	60.45	178.52	-0.16
	0.5	3.15×10^{5}	69.40	181.87	-0.16	6.75×10^{5}	74.31	182.21	-0.15
	0.6	8.52×10^{7}	106.70	185.73	-0.11	1.29×10^{7}	109.55	186.12	-0.11
	0.7	3.12×10^{8}	118.36	189.85	-0.10	1.47×10^{8}	113.79	189.83	-0.10
	0.8	1.84×10^{6}	87.29	190.04	-0.14	1.41×10^{6}	85.65	190.00	-0.14
	0.9	1.16×10^{4}	55.40	189.52	-0.19	1.02×10^{4}	54.64	189.53	-0.19
Average		$\mathbf{4.44 \times 10^{7}}$	**69.45**	-	-	$\mathbf{3.09 \times 10^{7}}$	**70.95**	-	-

Table 5. Kinetic and thermodynamic parameters with percentage error between neuron numbers 5 and 12 from FWO - *LL* kinetic model.

Kinetic model					**FWO - *LL***					
Parameters	α	R^2		%Error	E_a (kJ/mol)		%Error	A (s^{-1})		%Error
Source		**[5 5]**	**[12 12]**		**[5 5]**	**[12 12]**		**[5 5]**	**[12 12]**	
M/HDPE/Bifunctional HZSM-5/LS	0.1	0.9134	0.8948	2.08	46.07	42.80	7.63	5.48×10^3	2.67×10^3	105.74
	0.2	0.9600	0.9600	0.00	53.35	53.35	0.00	2.22×10^4	2.22×10^4	0.00
	0.3	0.8861	0.8893	0.36	59.02	58.68	0.58	5.06×10^4	4.77×10^4	6.00
	0.4	0.8227	0.8287	0.72	66.04	66.00	0.05	1.15×10^5	1.17×10^5	1.34
	0.5	0.6683	0.6683	0.00	80.27	80.27	0.00	6.75×10^5	6.75×10^5	0.00
	0.6	0.9372	0.9356	0.17	114.68	115.80	0.97	1.08×10^8	1.29×10^7	15.91
	0.7	0.9660	0.9623	0.38	119.53	120.32	0.66	1.31×10^8	1.47×10^8	10.90
	0.8	0.8697	0.8620	0.89	95.44	92.51	3.17	2.17×10^6	1.41×10^6	54.00
	0.9	0.5556	0.6021	7.72	62.59	62.35	0.38	1.06×10^4	1.02×10^4	3.27
Parameters	α	ΔH (kJ/mol)		%Error	ΔG (kJ/mol)		%Error	ΔS (kJ/mol K)		%Error
Source		**[5 5]**	**[12 12]**		**[5 5]**	**[12 12]**		**[5 5]**	**[12 12]**	
M/HDPE/Bifunctional HZSM-5/LS	0.1	41.52	38.23	8.60	177.00	178.08	0.61	-0.19	-0.19	3.12
	0.2	48.44	48.44	0.00	175.86	175.86	0.00	-0.18	-0.18	0.00
	0.3	53.80	53.47	0.63	176.57	176.58	0.01	-0.17	-0.17	0.28
	0.4	60.47	60.45	0.04	178.64	178.52	0.06	-0.16	-0.16	0.08
	0.5	74.31	74.31	0.00	182.21	182.21	0.00	-0.15	-0.15	0.00
	0.6	108.43	109.55	1.02	186.04	186.12	0.04	-0.11	-0.11	1.36

Kinetic model		**FWO - *LL***								
Parameters	α	R^2		%Error	E_a (kJ/mol)		%Error	$A\ (s^{-1})$		%Error
Source		**[5 5]**	**[12 12]**		**[5 5]**	**[12 12]**		**[5 5]**	**[12 12]**	
	0.7	113.00	113.79	0.69	189.73	189.83	0.05	-0.11	-0.10	0.91
	0.8	88.59	85.65	3.43	190.33	190.00	0.17	-0.14	-0.14	2.50
	0.9	54.88	54.64	0.45	189.57	189.53	0.02	-0.19	-0.19	0.15
Average		**71.49**	**70.95**	**1.65**	**-**	**-**	**0.11**	**-**	**-**	**0.93**

Table 6. Mean absolute error across different empirical reaction model across different weight loss, α in an averaging range of heating rate.

No	Equation	Empirical parameters				Min MAPE (%)
		n	*m*	*p*	*d*	
E.1	$(1-\alpha)^n \,.\, \alpha^m .\ p\left[\alpha^{\frac{(p-1)}{p}}\right] .\frac{1}{2}\,(\alpha)^{-d}$	21.09	47.62	14.61	-42.47	56.65
E.2	$3(1-\alpha)^{\frac{2}{3}} .\ \alpha^n .\ m\left[\alpha^{\frac{(m-1)}{m}}\right] .\frac{1}{2}\,(\alpha)^p$	4.35	16.94	61.38	-	80.00
E.3	$3(1-\alpha)^{\frac{2}{3}} .\ \alpha^n .\ \ [-\ln(1-\alpha)]^{-m}$	48.66	-43.72	-	-	55.91
E.4	$(1-\alpha)^n \,.\, \alpha^m .\ p(1-\alpha)[-\ln(1-\alpha)]^{\frac{p-1}{p}}$	-11.38	46.52	77.75	-	80.00
E.5	$(1-\alpha)^n \,.\, \alpha^m .\ p(1-\alpha)[-\ln(1-\alpha)]^{\frac{p-1}{p}} .\frac{1}{2}\,(\alpha)^d$	20.85	-23.64	38.22	29.31	51.80
E.6	$3(1-\alpha)^{\frac{2}{3}} .\ \alpha^n .\ \ m(1-\alpha)[-\ln(1-\alpha)]^{\frac{m-1}{m}}$	35.57	0.03	-	-	78.46

E.7	$3(1-\alpha)^{\frac{2}{3}}.\ \alpha^{n}.\ \ m(1-\alpha)[-\ln(1-\alpha)]^{\frac{m-1}{m}}.\frac{1}{2}\ (\alpha)^{p}$	21.47	0.03	14.26	-	56.32
E.8	$(1-\alpha)^{n}.\ \alpha^{m}.\ p\left[\alpha^{\frac{(p-1)}{p}}\right].\frac{d}{2}\left[(1-\alpha)^{-\frac{1}{d}}-1\right]^{-1}$	24.56	10.42	69.24	-8.88	60.85
E.9	$(1-\alpha)^{n}.\ \alpha^{m}.\ p\ (1-\alpha)[-\ln(1-\alpha)]^{\frac{p-1}{p}}.\frac{d}{2}\left[(1-\alpha)^{-\frac{1}{d}}-1\right]^{-1}$	21.62	6.36	37.40	-1.49	65.37
E.10	$3(1-\alpha)^{\frac{2}{3}}.\ \alpha^{n}.\ m\left[\alpha^{\frac{p-1}{p}}\right].\frac{3}{2}[(1-\alpha)^{-\frac{1}{3}}-1]^{-1}$	29.22	42.83	-	-	80.00
E.11	$(1-\alpha)^{n}.\ \alpha^{m}.\ p\left[\alpha^{\frac{(p-1)}{p}}\right].\ \frac{3}{2}[(1-\alpha)^{-\frac{1}{3}}-1]^{-1}$	22.18	7.78	22.28	-	**51.59**
Siddiqi et al. (2021)	$(1-\alpha)^{n}.\ \alpha^{m}.\ [-\ln(1-\alpha)]^{-p}$	1.09	44.57	- 40.43	-	67.90

Highlights

- Synergistic effect of catalytic co-pyrolysis of M/HDPE were evaluated.
- ANN model was established to generate the weight loss data of samples.
- FWO model gave the best prediction for kinetic parameters.
- The E_a range of M/HDPE/ Bifunctional HZSM-5/LS was reduced to 75.37 – 76.90 kJ/mol.
- Empirical model with a MAPE of 51.59% was developed.